

Rotation in Gravitational Lenses

Ue-Li Pen^{1,2}, Shude Mao³ \star

¹ *National Astronomical Observatories, Chinese Academy of Sciences, A20 Datun Road, 100012 Beijing, China*

² *Canadian Institute for Theoretical Astrophysics, 60 St. George St., Toronto, M5S 3H8, Canada*

³ *University of Manchester, Jodrell Bank Observatory, Macclesfield, Cheshire SK11 9DL, UK*

Accepted Received; in original form

ABSTRACT

Gravitational lensing deflects light. A single lens deflector can only shear images, but cannot induce rotations. Multiple lens planes can induce rotations. Such rotations can be observed in quadruply imaged sources, and can be used to distinguish between two proposed solutions of the flux anomaly problem: substructures in lensing galaxies vs large scale structure. We predict the expected amount of rotation due to large scale structure in strong lensing systems, and show how this effect can be measured using \sim mas VLBI astrometry of quadruple lenses with extended source structures. The magnitude of rotation is around one degree. The biggest theoretical uncertainty is the power spectrum of dark matter on very small scales. This procedure can potentially be turned around to measure the dark matter power spectrum on very small scales. We list the predicted RMS rotation angles for several quadruple lenses with known lens and source redshifts.

Key words: gravitational lensing - cosmology: theory - dark matter - galaxies: structure, evolution

1 INTRODUCTION

Gravitational lensing results from the deflection of light under the gravitational influence of all matter, luminous or otherwise. Its physics is clean, and this effect has allowed the measurement of the distribution of dark matter from galaxy-scales (using strong lensing) to the large-scale structure of the universe (using weak lensing).

Usually, many approximations are made to simplify the calculations. One of these is the Born

\star upen@cita.utoronto.ca; smao@jb.man.ac.uk

approximation, where one calculates a small deflection along the unperturbed light path. Some effects, such as image rotation due to multi-plane lensing, are not accessible in this approximation. Authors have obtained different results for the magnitude of multi-plane weak lensing rotation (Jain et al 2000, Cooray & Hu 2002, hereafter CH; Hirata & Seljak 2003, hereafter HS). Schneider (1997) showed that a strong lens plus spatially constant weak lens system is mathematically identical to some other single lens plane system, so only differential rotation at the image positions is observable.

In this paper, we apply the multiple plane lensing calculation to real physical systems: quadruply imaged quasars. We show in this physical example how the rotation effect can be measured, why it is physical and real, estimate its magnitude, and show how it can be used to resolve the substructure controversy.

The rotation of images is of current interests in the context of using gravitational lensing to detect substructures predicted by the Cold Dark Matter (CDM) structure formation model. From both semi-analytical studies and numerical simulations, it became clear that hundreds of subhaloes (substructures) are predicted to exist in a Milky-Way type halo (e.g., Kauffmann et al. 1993; Klypin et al. 1999; Moore et al. 1999; Ghigna et al. 2000). In general, about 5-10% of the mass is predicted to be in substructures, with a typical mass spectrum of $n(M)dM \sim M^{-1.8}dM$. If all the substructures form stars, then the predicted number of satellite galaxies exceeds the observed number in a Milky-Way type halo by a large factor. It is now, however, clear that the correspondence between substructures and visible satellite galaxies is not simple (Gao et al. 2004a,b; see also Springel et al. 2001; Diemand, Moore & Stadel 2004; Nagi & Kravtsov 2005). In particular, if only some substructures house satellite galaxies, then the discrepancy can be alleviated (e.g., Kravtsov et al. 2004). At present, it is not entirely clear whether the internal kinematics of satellite galaxies are consistent with observations (Stoehr et al. 2002; Kazantzidis et al. 2004). Furthermore, the spatial distribution of satellite galaxies in the Milky Way is also somewhat puzzling (Kroupa et al. 2004, but see Kang et al. 2005; Liebeskind et al. 2005; Zentner et al. 2005).

One possible way to detect the (dark) substructures is through the gravitational lensing effect. Simple analytical models in gravitational lenses often fail to reproduce the observed flux ratios (e.g., Kochanek 1991). This discrepancy is commonly referred to as the “anomalous flux ratio problem.” This has been proposed as evidence for substructures in the primary lensing galaxies (e.g., Mao & Schneider 1998; Metcalf & Zhao 2002; Dalal & Kochanek 2002). However, as most of the predicted substructures are in the outer part of the lensing galaxies while the lensed images are typically at a projected distance of only a few kpc from the center, it is unclear whether the

predicted amount of substructures in lensing galaxies by CDM is sufficient (Kochanek & Dalal 2004; Mao et al. 2004), so it is important to consider other sources of “substructures.” Recently, Metcalf (2005) proposed that substructures along the line of sight can equally explain the discrepancy. A key question naturally arises: how do we know that substructures are from the primary lens or from elsewhere along the line of sight?

In this paper, we examine the rotation of images induced by structures along the line of sight in gravitational lenses (see also Chen et al. 2003). We use a novel power-spectrum approach and consider the fluctuations of surface densities among different images (separated by few tenths to few arc seconds) and their effects on the magnifications. Throughout this paper, we adopt the “concordance” Λ CDM cosmology (e.g., Ostriker & Steinhardt 1995; Spergel et al. 2003 and references therein), with a density parameter $\Omega_m = 0.3$, a cosmological constant $\Omega_\Lambda = 0.7$, a baryon density parameter $\Omega_b = 0.024h^{-2}$, and the power-spectrum normalization $\sigma_8 = 0.9$. We adopt a Hubble constant of $H_0 = 70 \text{ km s}^{-1} \text{ Mpc}^{-1}$.

2 LENSING BY LARGE SCALE STRUCTURE IN THE PRESENCE OF A STRONG LENS

Many multiply-imaged gravitational lenses on galaxy-scales have been observed. At the time of writing, roughly 100 such systems are known¹. The largest systematic survey, the Cosmic Lens All Sky Survey (CLASS) has found 22 new galaxy-scale lenses, approximately one half of which are quadruple lenses (Browne et al. 2003; Myers et al. 2003). Most of these have high-resolution imaging from 0.1'' to mas from MERLIN, HST to VLBI. Several of these lenses are resolved into multiple components. The system 0128+437 provides a good example (Biggs et al. 2004). Each of the image has been resolved into three sub-components with VLBI. Such high-resolution images provide an excellent test bed for lensing models.

In addition to the strong lens system which causes the multiple image splitting, all the matter along the line of sight will further deflect the light and contribute to distortions in the image. One such effect is the apparent rotation of images. It can be shown that a single plane lens has a symmetric amplification matrix, which shears but does not rotate images. With multiple planes, image rotation is possible. Observing it may appear non-trivial, since it would require prior knowledge of the unlensed image alignment. We will show below (see §3) how this can actually be measured if one has a quadruply imaged source with extended structures.

¹ see the CaSTLES database: <http://cfa-www.harvard.edu/castles/>

Several geometric configurations can lead to image rotation. A strong lens has shear and convergence of order unity. With sufficiently accurate alignment, a second strong lens could occur along the line of sight. Indeed such an example has already been seen – the JVAS/CLASS lens system, B2114+022 (Augusto et al. 2001; Chae, Mao & Augusto 2001), has two lensing galaxies at redshifts 0.3157 and 0.5883 respectively, within 2 arc seconds of quadruple radio sources².

But in general, the expected variation in surface density due to dark matter is small. Integrating the Limber equation, this leads to large scale structure density variations of order a few percent of the critical surface density (e.g., Jain et al 2000). So a random cluster lens will typically only have weak lenses in its foreground and background.

The typical splitting angle of the strong lens is around one arc second. Large scale structure density fluctuations on such scales are significantly correlated. Since Schneider (1997) had shown that perfectly correlated weak lensing screens do not cause observable rotation, one must compute the differential weak lensing shear.

The cross correlation between two image positions separated by angle $\Delta\theta$ is defined as

$$r \equiv \xi_\kappa(\Delta\theta)/\xi(0), \quad (1)$$

where $\xi_\kappa(\Delta\theta)$ is the two dimensional Fourier (Bessel) transform of Equation (17) which will be discussed below. The results are shown for four quadruple lenses with known lens and source redshifts, B1422+231 (Patnaik et al. 1992), MG0414+0534 (Hewitt et al. 1992), B1608+656 (Myers et al. 1995), and B2045+265 (Fassnacht et al. 1999). We find a ratio of variances between the difference of two images σ_-^2 and the individual variances to be

$$\frac{\sigma_-^2}{\sigma^2} = 2(1 - r). \quad (2)$$

If the two images are uncorrelated, the difference will have twice the variances of each individual image. Figure 1 shows the correlation function vs. image separation. As can be seen, typically we have $r > 0.5$, so the difference mode has a slightly lower variance than each individual image.

We assume that the various images pass through different parts of the strong lens with correspondingly different values of shear and convergence, and also differing weak lens deflectors. We consider a 2-plane lens, L_1 is the strong lens, L_2 is a weak lens due to large scale structure, O is the observer position and S is the source plane. The geometry is shown in Figure 2. We consider a quadratic potential on each lens plane, $\phi = ax_1^2 + 2bx_1x_2 + cx_2^2$, where (x_1, x_2) are the (angular) coordinates in the lens plane. The units for the potential are chosen such that $2\kappa = \nabla^2\phi$, and the

² It is present unclear whether the radio sources B and C are lensed images.

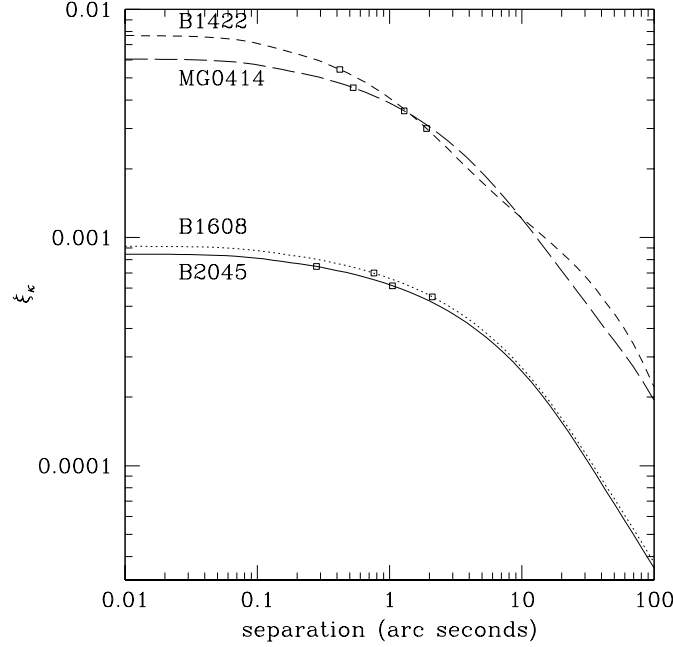


Figure 1. The correlation function for convergence (κ) for different image pairs induced by the large-scale structure; the correlation function at zero lag is the variance in κ . The boxes indicate the largest and smallest splittings for four CLASS lenses with known lens and source redshifts. Because splitting angles are small, the κ by the large-scale structure at different image positions is strongly correlated. The variance from large scale structure shear at each image position is the correlation function at zero lag. The covariance for images separated by a lag $\Delta\theta$ can be seen in the plots. Since the covariance (at typical image separations) is of comparable size of to the auto-variance, which leads to a suppression of the differential shear mode.

deflection angle is $\hat{\alpha} = \nabla_x \phi$ due to lens, where we use the same notations as in Schneider, Ehlers, & Falco (1992). To distinguish the two lens planes, we will use a prime to denote variables in the L_2 plane.

For a general anisotropic lens, the deflection angle is a vector. For our quadratic potential, κ and $\gamma_{1,2}$ are constant on the plane,

$$\kappa = \frac{1}{2}(a + c), \quad \gamma_1 = \frac{1}{2}(a - c), \quad \gamma_2 = b. \quad (3)$$

The quadratic potential is the most general function which leads to constant values of κ and γ . Their constancy on small scales is inferred from the correlation function shown in Figure 1. In such a potential, the full gravitational lensing effect is straightforward to compute. One can solve the full photon trajectory, which are deflected on the lens planes by the gradient of the potential.

We now denote D_1 to be the angular diameter distance from the observer to the first lens, D_{12} the distance from the first to the second lens, and D_{2s} the distance from the second lens to the source, and so on. We see from Figure 1 that all the relative deflection angles are very small in units of radians ($\sim 10^{-5}$), so we can expand to first order in the deflection angle (Schneider et al. 1992, chapter 9)

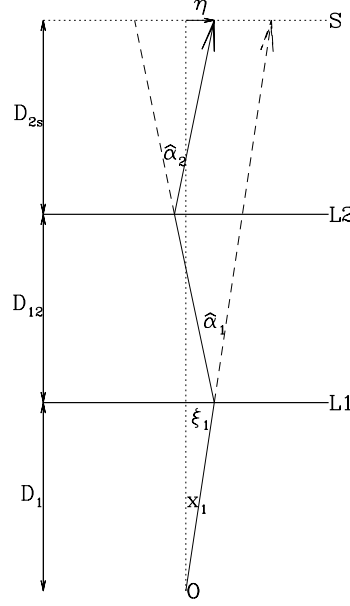


Figure 2. Lensing geometry. The deflection angles themselves are not observable, but rather the changes in deflection angle. Various quantities are indicated in the Figure and used in eqs. (4-7).

$$\eta = \frac{D_s}{D_1} \xi_1 - D_{1s} \hat{\alpha}_1(\xi_1) - D_{2s} \hat{\alpha}_2(\xi_2), \quad \xi_2 = \frac{D_2}{D_1} \xi_1 - D_{12} \hat{\alpha}_1(\xi_1). \quad (4)$$

where η , ξ_1 , ξ_2 denote the position vectors in the source plane and the first and second lens planes (see Fig. 2), and the deflection angles in the first and second planes are given as $\hat{\alpha}_1$ and $\hat{\alpha}_2$.

Following Schneider et al. (1992), we define two reduced deflection angles

$$\alpha_1 = \frac{D_{1s}}{D_s} \hat{\alpha}_1, \quad \alpha_2 = \frac{D_{2s}}{D_s} \hat{\alpha}_2, \quad (5)$$

With these, eq. (4) can be recast in a very simple form using only angles:

$$\mathbf{y} = \mathbf{x}_1 - \alpha_1(\mathbf{x}_1) - \alpha_2(\mathbf{x}_2), \quad \mathbf{x}_2 = \mathbf{x}_1 - \beta_{12} \alpha_1(\mathbf{x}_1), \quad (6)$$

where $\mathbf{y} = \eta/D_s$, $\mathbf{x}_1 = \xi_1/D_1$, $\mathbf{x}_2 = \xi_2/D_2$, and $\beta_{12} = D_{12}D_s/(D_2D_{1s})$.

Lensing shear and magnification can be obtained by studying the change of source position \mathbf{y} resulting from a change of apparent angular position \mathbf{x}_1 . In particular, the magnification is given by (Schneider et al. 1992)

$$\mathbf{A} = \frac{\partial \mathbf{y}}{\partial \mathbf{x}_1} = \mathcal{I} - \mathbf{U}_1 - \mathbf{U}_2 + \beta_{12} \mathbf{U}_2 \mathbf{U}_1, \quad (7)$$

where \mathcal{I} is a unit matrix, $\mathbf{U}_1 = \partial \alpha_1 / \partial \mathbf{x}_1$, and $\mathbf{U}_2 = \partial \alpha_2 / \partial \mathbf{x}_2$.

We are considering the combined effects of a strong and a weak lens. The contribution of the weak lens \mathbf{U}_2 is small and we are only interested in its contribution to rotation, so we neglect its linear effect. In the linear (i.e. Born approximation) regime, it is also observationally not possible

to distinguish between contributions from the strong and weak lens. In the product term, we can absorb β_{12} into the definition of U_2 . We define the critical density for the weak lensing large scale structure to be

$$\Sigma_2^{\text{crit}} \equiv \frac{c^2}{4\pi G} \frac{D_{1s}}{D_{12}D_{2s}}, \quad (8)$$

which is the lensing strength of the large scale structure as seen by an observer at the strong lens position. This lends a simple observational and computational interpretation of lensing rotation: all distortions visible to an observer at the strong lens position enter linearly into the coupling product of strong and weak lens.

An analogous results holds when the weak lensing plane is in front of the strong lens. In our notation, we have

$$\mathbf{U}_1 = \begin{pmatrix} \kappa + \gamma_1 & \gamma_2 \\ \gamma_2 & \kappa - \gamma_1 \end{pmatrix}, \quad \mathbf{U}_2 = \begin{pmatrix} \kappa' + \gamma'_1 & \gamma'_2 \\ \gamma'_2 & \kappa' - \gamma'_1 \end{pmatrix} \quad (9)$$

where $\kappa' \equiv \Sigma_2/\Sigma_2^{\text{crit}}$, and so

$$\begin{aligned} \mathbf{A} &= \begin{pmatrix} \gamma_2\gamma'_2 + (1 - \kappa + \gamma_1)(1 - \kappa' + \gamma'_1) & \gamma'_2(1 - \kappa - \gamma_1) + \gamma_2(1 - \kappa' + \gamma'_1) \\ \gamma'_2(1 - \kappa + \gamma_1) + \gamma_2(1 - \kappa' - \gamma'_1) & \gamma_2\gamma'_2 + (1 - \kappa - \gamma_1)(1 - \kappa' - \gamma'_1) \end{pmatrix} \\ &\sim \begin{pmatrix} 1 - \kappa + \gamma_1 & \gamma_2 + \gamma_2\gamma'_1 \\ \gamma_2 - \gamma_2\gamma'_1 & 1 - \kappa - \gamma_1 \end{pmatrix}. \end{aligned} \quad (10)$$

In the last approximate equality we used the limit that the weak lensing plane (the primed variables) are much smaller than the strong lens plane, but keeping the anti-symmetric piece which is relevant for rotations. We define the off-diagonal antisymmetric component as $\omega \equiv \gamma_2\gamma'_1$.

For strong lens systems, the shear on L_1 is of order unity, while the large-structure shear (γ'_1 , γ'_2) is a few percent, corresponding to a rotation of order a degree. Rotation only results when the principal axes of the two amplification matrices are misaligned. We choose the coordinates such that

$$\mathbf{U}_1 = \begin{pmatrix} \gamma & 0 \\ 0 & -\gamma \end{pmatrix}, \quad \mathbf{U}_2 = \begin{pmatrix} \gamma'_1 & \gamma'_2 \\ \gamma'_2 & -\gamma'_1 \end{pmatrix}. \quad (11)$$

γ'_1 does not contribute to rotation, so we set it to zero. Their product is a pure antisymmetric matrix

$$\mathbf{U}_2\mathbf{U}_1 = \begin{pmatrix} 0 & \gamma\gamma'_2 \\ -\gamma\gamma'_2 & 0 \end{pmatrix}. \quad (12)$$

When added to a unit matrix, this corresponds to a rotation matrix by an angle $\gamma\gamma'_2$.

In equation (10), we factor the amplification matrix $\mathbf{A} = \mathbf{A}_s\mathbf{R}(\phi)$, as a product of a symmetric matrix and a pure rotation, where the rotation matrix

$$\mathbf{R} = \begin{pmatrix} \cos \phi & \sin \phi \\ -\sin \phi & \cos \phi \end{pmatrix}. \quad (13)$$

We have

$$\mathbf{A} = \begin{pmatrix} 1 - \kappa + \gamma_1 & \gamma_2 + \omega \\ \gamma_2 - \omega & 1 - \kappa - \gamma_1 \end{pmatrix}, \quad (14)$$

where ω indicates the importance of rotation. Then we find

$$\tan \phi = -\frac{\omega}{1 - \kappa}. \quad (15)$$

The non-rotating amplification matrix \mathbf{A}_s has the same convergence as \mathbf{A} up to $O(\omega^2)$, but has its shear components rotated by $\phi/2$.

The different images pass through different parts of the strong lens, each with its own values of shear γ . The rotation angle will thus be different for each image. The actual value of the large scale structure shear depends on the non-linear power spectrum of dark matter at small physical scales. This is both a function of the primordial power spectrum and its slope, and non-linear gravitational physics. The most accurate models seem to be a combination of N-body simulations and heuristic models based on stable clustering. Calibrations at larger scales indicate consistency at the better than 20% level on length scales larger than about 100 kpc. In the standard models, the contribution from smaller scales is not dominant, so one would expect forecasts to be good to a factor of two (Huffenberger & Seljak 2003).

To forecast the expected RMS rotation angle, we compute the expected differential variation in the weak lens screen shear, and apply to eqs. (12,15). Mathematically, shear is a polarization field, which can be described as a trace-free spin-2 tensor field. In two spatial dimensions, any trace-free spin-2 tensor field can be decomposed into two kinematic scalars: the “divergence-like” component, also known as “E”-mode which is longitudinal to its Fourier decomposed wave vector, and a pseudo-scalar “curl-like” or “B”-mode which is transverse to its wave vector. In weak gravitational lensing, the “E”-mode is identical to the convergence field κ , and the “B”-mode is zero. To compute the statistics of the shear, it thus suffices to calculate the dimensionless variations in projected matter surface density. Its variation is given by the Limber equation. It involves the projection of a three dimensional non-linear power spectrum

$$\Delta^2(k, z) \equiv \frac{k^3}{2\pi^2} P(k, z) \quad (16)$$

to a two dimensional angular power spectrum $l(l+1)C_l/2\pi$ (Limber 1954; Kaiser 1992, 1998),

$$\frac{l(l+1)}{2\pi} C_l = \frac{\pi}{l} \int_{z_i}^{z_f} \Delta^2(l/\Delta\chi(z), z) w(z)^2 \chi(z) \frac{d\chi}{dz} dz. \quad (17)$$

For the foreground large scale structure, $z_i = 0$, $z_f = z_l$, $\Delta\chi(z) = \chi(z)$ where z_l is the redshift of the strong lens. For the background large scale structure, $z_i = z_l$, $z_f = z_s$, $\Delta\chi(z) = \chi(z_f) - \chi(z)$, where z_s is the source redshift. We used the Peacock and Dodds (1996) formulation to obtain the non-linear power from the linear transfer function given by Bardeen et al (1986). The comoving angular diameter distance is

$$D_A \equiv \chi(z) = c \int_0^z \frac{dz}{H(z)} \quad (18)$$

where $H(z)$ is the Hubble constant at redshift z :

$$H(z) = H_0[(1+z)^2(\Omega_m z + 1) - \Omega_\Lambda z(z+2)]^{1/2}. \quad (19)$$

For the comoving angular diameter distance χ we used the fitting formula from Pen (1999). In a cosmological context, it is convenient to use comoving angular diameter distances and conformal time, where light rays propagate as they do in an empty universe (White & Hu 2000). The lensing weight is

$$w(z) = \frac{3}{2}\Omega_m H_0^2 g(z)(1+z) \quad (20)$$

where

$$g(z) = \frac{[\chi(z_f) - \chi(z)][\chi(z) - \chi(z_i)]}{\chi(z_f) - \chi(z_i)}. \quad (21)$$

In terms of our previous variables, for the background weak lenses we have $D_{12} = \chi(z) - \chi(z_l)$, $D_{2s} = \chi(z_s) - \chi(z)$, etc. The lensing weighting factor g corresponds to the distance weighted terms in Equation (8). A similar relation holds for the background lenses.

Table 1 gives the expected rotation angle for a variety of quadruple lenses in the Λ CDM cosmology. Several simplifying assumptions were made. We attribute all the rotation to the furthest image. The change in strong lens γ between images is taken to be 0.3, which is multiplied by the large scale structure shear in equation (12). What matters is not the change in the absolute value of γ , but the change in each component. We took the variance of the large scale structure shear to be half of the convergence, which corresponds to the variance in γ_2 in the principal axis frame of the strong lens. In practice, only differences in rotation angles are observable, which depends on the alignment angles of the shear at different image positions. There is a contribution to rotation from the structure in the foreground as well as the background of the lens. The variances were simply added. The ratio of the foreground to background variance is listed in column 5 in Table 1. With all these caveats, we expect the expected rms image rotation to be good to about a factor of two, which is comparable to the expected errors on the theoretical lensing power spectrum.

lens	z_{lens}	z_{source}	κ_+	κ_-	$\Delta\phi$ (rms $^\circ$)	$(< z_{\text{lens}})/(> z_{\text{lens}})$
B2045+265	0.87	1.28	0.018	0.003	0.4	35
B0712+472	0.41	1.34	0.0076	0.014	0.39	0.29
B1608+656	0.63	1.39	0.015	0.010	0.44	2.4
MG0414+0534	0.958	2.64	0.030	0.021	0.9	2.0
B1422+231	0.34	3.62	0.007	0.049	1.2	0.02

Table 1. Expected image rotation angle for the most magnified image. We assumed a characteristic change in strong lens γ of 0.3 between images, and $\kappa = 0.5$ at each image position. Listed are the lens and source redshifts, the expected rotation angle, and the ratio of variances contributed from foreground compared to background large scale structure. κ_+ is the standard deviation of κ and γ due to foreground large scale structure, while κ_- is the contribution of the background.

3 MEASURING ROTATION

We only consider the simplest case. The source is made up of three components, P^1, P^2, P^3 . We define P^3 to sit at the origin, P^2 to sit at (P_x^2, P_y^2) , and P^1 at (P_x^1, P_y^1) . We can always choose our coordinate system this way.

The lensed image appears at positions A, B, C, D also with three components each. We again define the position of the third component to be the origin, and only consider relative distances. The apparent position of A^2 relative to A^3 is $P^2 = \mathbf{D}_A A^2$, and similarly $P^1 = \mathbf{D}_A A^1$ where the deflection matrix \mathbf{D}_A is the inverse of the amplification matrix \mathbf{A} defined in equation (7) for image A; each image has its own deflection matrix. It will be convenient to concatenate the two position column vectors P^1, P^2 into a 2×2 matrix \mathbf{P} . We can write similar equations for all images, resulting in an apparent 16 equations for 16 unknowns: \mathbf{P} each has four unknowns, and each symmetric amplification matrix has three unknowns. The equations are linear, and homogeneous:

$$\mathbf{D}_A \mathbf{A} = \mathbf{P}, \quad \mathbf{D}_B \mathbf{B} = \mathbf{P}, \quad \mathbf{D}_C \mathbf{C} = \mathbf{P}, \quad \mathbf{D}_D \mathbf{D} = \mathbf{P}. \quad (22)$$

It is clear that one could multiply each solution by a constant and obtain a solution, so one must fix one more parameter. Without loss of generality, one could fix $P_x^2 = 1$, which just fixes a length scale. If none of the amplifications are known, the solutions are clearly degenerate between a small image that is strongly magnified and a larger image that is less magnified. A further degeneracy occurs because we can multiply each equation on the left by an arbitrary shear matrix. Since we do not know the intrinsic location of the source substructure positions, this is indistinguishable from a constant shear applied to both the lens and the source. This corresponds to a shear plane between strong lens and source. For a shear between observer and strong lens, one can similarly symmetrize the deflection matrix by multiplying both the lens and the sources by the inverse shear matrix. This is in accordance with Schneider (1997). Thus, we only measure the differences in shears at the image positions.

Then we have 16 equations for 15 unknowns, which is over-determined by one. This allows us

to solve for one rotation angle. If one assumes the rotation to be dominated by the most magnified image, say A , we simply allow \mathbf{D}_A to be non-symmetric. This allows one to solve for the rotation angle.

In general, however, the large scale structure shear has two independent components γ_1, γ_2 . To make progress, one can assume them to be Gaussian distributed with standard deviation σ . Their one point function is independent, $P(\gamma_1, \gamma_2) = N(\gamma_1, \sigma)N(\gamma_2, \sigma)$. Equation (12) expresses the off-diagonal components of each deflection matrix in terms of the two large-scale structure shear components. If we fix a value of γ_1 , we can solve Equation (22) for γ_2 , giving us an implicit definition of $\gamma_2(\gamma_1)$. Then integrating over all possible values of γ_1 weighted by the probability gives the total likelihood for an assumed σ :

$$L(\sigma) = \int P(\gamma_1, \gamma_2(\gamma_1)) d\gamma_1. \quad (23)$$

One can then solve for the maximum likelihood value of σ .

4 DISCUSSION

If one wishes to observe this effect, several challenges must be overcome. Sources must have at least three localizable components, and the position of each must be measured very precisely, to better than 1% of the component separation. Positions are also affected by changes in the lens from one component position to the next. The latter effect is expected to be significantly smaller than rotation, because it depends on the change in shear on small scales, while the rotation depends on the large scale structure shear itself. Basically, the rotation is of order of the large scale structure shear. The variation of the large scale structure shear on source substructure scales is smaller than the shear itself.

We quantify this as follows: let us assume that the components of the lens have a separation of 10 mas. The model assumed that the shear was constant over the apparent size of the source. The change in shear across the lens is given by $\xi_\kappa(\Delta\theta = 10\text{mas})$. From Figure 1 we see that κ has a differential variance of around 10^{-4} at this separation, corresponding to a percent change in lensed length scales. This is of comparable magnitude to the rotation effect, which makes it desirable to have more than three components to check. In practice, the actual lensing substructure is suppressed by several factors. Figure 1 shows the weak lensing correlation in the absence of a strong lens. Lines converge behind the lens, which reduces the corresponding physical scales, and thus the total variance. And only the variation in shear principle axes across three sub-image positions affects the rotation, which is suppressed by another dimensionless factor.

It is worth noting that HS proved that the rotation ω is identical to the B-mode of the shear, up to a constant. In this calculation, we only considered the local value of shears, while the E-B decomposition is non-local. We therefore should consider the 4 entries in the magnification matrix to be independent. In principle, if one had a very high number density of background sources, for example from reionization (Pen 2004), one could also solve for the strong lensing E-B decomposed map (Pen 2000). Such a decomposition also allows one to distinguish between structures in the strong lens plane, and contributions from large scale structure along the line of sight. The signal to noise required for such an exercise is difficult to achieve with current technology. Using quadruply imaged sources allows one to reduce the pairwise noise, and thus solve for the rotational component.

We also note that our calculation did not use the Born approximation. We modeled each lens plane by a quadratic potential as inferred from the κ correlation function, and computed the full deflection trajectories. Recently, calculations of rotations by large scale structure at different lens planes resulted in different answers, depending on whether calculations were done with light rays (HS) or with shears on light bundles (CH). In the CH calculation, ray bundles were propagated on unperturbed trajectories, but distortions were accumulated. The distortions are relative deflections of neighboring rays, which accumulate rotations through the same effect as discussed in this paper. This allows CH to see rotation without considering the explicit deflection of the centers of each ray. In terms of a full Taylor expansion of light rays along unperturbed paths, this includes some of the effects beyond the Born approximation. HS included all leading order corrections to the Born approximation, and thus differed in their answer. In our case, the angular scales involved are very small, and we can assume the rotation to be dominated by the common large scale structure shear at different image positions. The CH and HS approaches do not differ in our model, since the potential is taken to be quadratic, and all second derivatives are constant.

Our result differ from that of Schneider (1997) in the nature of the effect. Schneider (1997) constructs an equivalent single plane strong lens from a strong lens plus constant weak shear. Our calculation circumvents the assumption that the weak lens screen is spatially constant.

Our model assumes a source plane consisting of three compact components with unknown positions. If all three components are quadruply lensed, there are a total of 12 angular positions, i.e., we have 24 observables. We subtract 8 degrees of freedom for the global lens model, because we do not know the macroscopic lens deflection angle. This leaves 16 constraints. Then using Equation (22) we can solve for the relative positions in the source plane modulo a scaling (due to the mass sheet degeneracy), which is three numbers, as well as the values of the amplification matrix

at each image position, which is four sets of 3 numbers, plus one rotation, for a total of 16 parameters. This suggests that small scale structure in a single lens is observationally distinguishable from weak shear at a different redshift.

We have made several approximations, which will affect the results at some level. We used the difference in shears at the two furthest image positions. In the analysis, we then assumed that three of the images had no rotation, and only the furthest accounted for the multi-plane rotation. Reality is more complex, and all images have differential weak lensing shear, and thus some level of differential rotation. Simulations are needed to quantify this simplifying assumption.

In this paper, we have concentrated on the rotation induced by the weak large-scale structure. However, for the cases where one has multiple lenses along the line of sight, the rotation can be more significant. For the best-fit model in Chae, Mao & Augusto (2001), we find that the two Jacobian matrices are given by

$$J = \begin{bmatrix} 0.176 & -0.093 \\ -0.258 & -0.595 \end{bmatrix}, \quad \begin{bmatrix} 0.888 & -0.174 \\ -0.148 & 0.481 \end{bmatrix}, \quad (24)$$

for images A and D, corresponding to magnifications -7.78 and 2.49 respectively. Clearly for the more highly magnified image A, the Jacobian is highly asymmetric and the rotation is quite significant.

5 CONCLUSIONS

We have computed the expected rotation from uncorrelated foreground and background large scale structure in strong lensing systems. We have shown that this effect is in principle observable with precise VLBI imaging of quadruply imaged lens systems. The rotation is physical and observable in the example of a source plane consisting of three point sources. If observed, it can unambiguously determine if the flux anomaly problem is caused by substructure on the lens plane, or by uncorrelated structures along the line of sight.

In addition, it demonstrates how one can extract information about small scale dark matter structure along the line of sight to a lens. A measurement of rotation would measure the variance of κ from large scale structure at the smallest scales. This affects the scatter in supernovae lensing effects, and may have potential to measure the primordial power on small scales, and possibly a tilt or running spectral index.

We thank Peter Schneider for pointing out a flaw in an earlier version of the paper, T. York and K.-H. Chae for helpful discussions, and Pengjie Zhang for the lensing Limber code.

REFERENCES

- Bardeen, J. M., Bond, J. R., Kaiser, N., Szalay, A. S 1986, ApJ, 304, 15
- Biggs, A. D., Browne, I. W. A., Jackson, N. J., York, T., Norbury, M. A., McKean, J. P., Phillips, P. M. 2004, MNRAS, 350, 959
- Bradac, M., Schneider, P., Steinmetz, M., Lombardi, M., King, L. J., Porcas R. 2002, A&A, 388, 373
- Browne, I.W.A., et al. 2003, MNRAS, 341, 13
- Cooray, A. and Hu, W. 2002, ApJ, 574, 19 (CH)
- Dalal, N., & Kochanek, C. S. 2002, ApJ, 572, 25
- Diemand, J., Moore, B., & Stadel, J. 2004, MNRAS, 352, 535
- Fassnacht, C. D. et al. 1999, AJ, 117, 658
- Gao, L., De Lucia, G., White, S. D. M., Jenkins, A., MNRAS, 2004a, 352, L1
- Gao, L., White, S. D. M., Jenkins, A., Stoehr, F., Springel, V., MNRAS, 2004b, 355, 819
- Ghigna, S., Moore, B. Governato, F., Lake, G., Quinn, T., Stadel, J. 2000, ApJ, 544, 616
- Hewitt, J. N., Turner, E. L., Lawrence, C. R., Schneider, D. P., Brody, J. P. 1992, AJ, 104, 968
- Hirata, C., & Seljak, U. 2003, PRD, 68, 083002 (HS)
- Huffenberger, K. M. & Seljak, U. 2003, MNRAS, 340, 1199
- Jain, B., Seljak, U. & White, S.D.M 2000, ApJ, 530, 547.
- Kaiser, N. 1992, ApJ, 388, 272
- Kaiser, N. 1998, ApJ, 498, 26
- Kauffmann, G., White, S. D. M., Guiderdoni, B. 1993, MNRAS, 264, 201
- Kazantzidis, S., Mayer, L., Mastrogiuseppe, C., Diemand, J., Stadel, J., Moore, B. 2004, ApJ, 608, 663
- Klypin, A., Kravtsov A. V., Valenzuela O. 1999, ApJ, 522, 82
- Kochanek, C.S. 1991, ApJ, 373, 354
- Kochanek, C.S., & Dalal, N. 2004, ApJ, 610, 69
- Kroupa, P., Theis, C., Boily, C. M., 2004, A&A, in press
- Liebskind, N. I., Frenk, C. S., Cole, S., Helly, J.C., Jenkins, A., Navarro, J. F., & Power, C. 2005, astro-ph/0503400
- Limber, D.N. 1954, ApJ, 119, 655
- Mao, S., Schneider, P. 1998, MNRAS, 295, 587
- Mao, S., Jing, Y. P., Ostriker, J. P., & Weller, J. 2004, ApJ, 604, L5
- Metcalf, R. B., & Zhao, H.S. 2002, ApJ, 567, L5
- Metcalf, R. B. 2005, ApJ, 622, 72
- Moore, B., Ghigna, S., Governato, F. et al. 1999, ApJ, 524, L19
- Myers, S. T. et al. 1995, ApJ, 447, L5
- Myers, S. T. et al. 2003, MNRAS, 341, 1
- Patnaik, A. R. et al. 1992, MNRAS, 259, 1P
- Nagai, D., Kravtsov A. V., 2005, ApJ, submitted, astro-ph/0408273
- Ostriker, J. P., & Steinhardt, P. J. 1995, Nature, 377, 600
- Peacock, J. A., & Dodds, S. J. 1996, MNRAS, 180, 19
- Pen, U. 1999, ApJS, 120, 49.
- Pen, U. 2000, ApJ, 534, L19
- Pen, U. 2004, New Astronomy, 9, 417
- Schneider, P., Ehlers, J. & Falco, E. 1992, "Gravitational Lenses", Springer Verlag.
- Schneider, P. 1997, MNRAS, 292, 673.
- Spergel, D.N.S. et al. 2003, ApJS, 148, 175
- Springel, V., White, S. D. M., Tormen, G., & Kauffmann, G. 2001, MNRAS, 328, 726
- Stoehr, F., White, S. D. M., Tormen, G., Springel, V. 2002, MNRAS, 335, L84

White, M & Hu, W 2000, ApJ, 537, 1

Zentner, A. R., Kravtsov, A. V., Gnedin, O. Y., & Klypin, A. A. 2005, astro-ph/0502496